Hindawi
Shock and Vibration
Volume 2019, Article ID 1219435, 9 pages
https://doi.org/10.1155/2019/1219435

Research Article

Experimental and Theoretical Analysis on the Dynamic Characteristics of Fused Filament Fabrication Plates

Shijie Jiang,[1] **Ming Zhan**,[2] **Mingyu Sun**,[1] **Weibing Dai**,[1] **and Chunyu Zhao**[1]

[1]*School of Mechanical Engineering and Automation, Northeastern University, Shenyang, China*
[2]*College of Information Science and Engineering, Northeastern University, Shenyang, China*

Correspondence should be addressed to Shijie Jiang; jiangsj@me.neu.edu.cn

Received 25 September 2019; Accepted 22 October 2019; Published 11 November 2019

Academic Editor: Vadim V. Silberschmidt

With the increasingly wide application of fused filament fabrication (FFF) technique, the built products are inevitably exposed to dynamic mechanical loading and vibration. However, there has been no systematic study in the literature on understanding and characterization of dynamic mechanical performance for FFF products. In this paper, the dynamic characteristics of FFF plates are quantified, with the effect of different extrusion width taken into account. A dynamic model of the built plate with cantilever boundary conditions is established, and the inherent characteristics are predicted. Modal tests are then performed on these samples to obtain the measured data. Through the comparison between predictions and measurements, the theoretical model is validated. Different extrusion width makes the material properties of the plates different, resulting in different dynamic characteristics. The scanning electron microscopy (SEM) analysis on the samples confirms that the dynamic characteristic is deteriorated as the extrusion width decreases. This present work provides theoretical basis and technical support for further research in improving the dynamic performance of FFF products and helps extend the applications of this technique.

1. Introduction

Fused filament fabrication (FFF), an extrusion-based additive manufacturing technique, is able to fabricate products almost without geometrical limitations [1, 2]. In this procedure, the raw material filament is first melted in an extrusion head. It is then extruded out from the nozzle that is moving in a scheduled mode. The molten filament cools, solidifies, and bonds with the extruded material layer beneath it. A three-dimensional model or product entity is finally completed by repeating this procedure to the last layer [3, 4]. It is a trend that FFF is used to produce end-use products for electronic, automotive, and aerospace applications. These products need to be repeatedly exposed to dynamic loading and vibration, and meanwhile they have to maintain high dynamic characteristic. Therefore, the analysis in terms of dynamic characteristic of FFF products is needed to accurately determine the reliability.

During the past few years, extensive research has been carried out in studying various quality characteristics of FFF products, such as mechanical property [5–8], surface roughness [9, 10], build quality [11–13], and dimensional quality [14, 15]. However, very few investigations have been performed on the built products' dynamic characteristics. Arivazhagan and Masood [16] used the DMA2980 equipment to conduct the frequency sweep test on FFF samples from 1 to 100 Hz to determine the modulus, damping, and viscosity values. The results illustrated that the strength of the product processed with solid built style was higher than those fabricated with other built styles. Increasing temperature would increase the products' loss modulus, but decrease the viscosity values and storage modulus. Mohamed et al. [17, 18] used the same test method to investigate different processing parameters' effect on the dynamic elastic modulus of samples and pointed out that modulus values would decrease when the build orientation, raster angle, or air gap increased. In addition, the numerical values of maximum glass transition temperature and dynamic modulus were determined by optimizing the processing parameters.

Although these studies were carried out under vibratory and cyclic conditions, the dynamic inherent characteristics of samples were not taken into account, i.e., natural frequency and mode shape. Furthermore, the above research was mainly relied on experimental testing, lacking theoretical basis and principle. For the first time, this paper established the theoretical model and carried out the experimental research to quantify different extrusion widths' influence on the FFF plates' inherent characteristics.

In this paper, the theoretical analysis of inherent characteristics of FFF plates is introduced first, followed by sample preparations and modal test research. The predicted and measured results are then analyzed to clarify the effect of different extrusion widths on the inherent characteristics of the plates. Scanning electron microscopy analysis is performed to identify the samples' characteristics in order to microscopically confirm the extrusion width effect.

2. Materials and Methods

To investigate the dynamic inherent characteristics of the FFF plates theoretically and experimentally, the modeling is introduced in this section first, followed by the fabrication of samples and the experimental tests.

2.1. Theoretical Model. The FFF plate, composed of multiple layers of fiber material made of polylactic acid (PLA, with the mechanical characteristics summarized in Table 1), has the characteristic of orthogonal anisotropy.

To model the plate, the following assumptions are made: (1) the layers are firmly bonded with each other, and there is no slip and no relative displacement between layers. Therefore, there is no need to consider the interlayer coupling effect. (2) The laminate plate can be regarded as an integral structural plate. The bonding layer is very thin, and no deformation occurs in itself, that is, the deformation between the single-layer plates is continuous. (3) The plate is composed of multiple single-layer plates, but the total thickness is still consistent with the thin plate assumption.

Figure 1 shows the geometric model of the rectangular plate, of which the length a is 130 mm, the width b is 50 mm, and the thickness h is 2.4 mm (the thickness of each single layer is the extrusion width of the extruded filament). Taking the central plane of the plate as the xoy plane, the three-dimensional coordinate system (O-xyz) was set up. The length, width, and thickness directions are separately represented by x, y, and z.

According to the small deflection theory of thin plates (Kirchoff hypothesis), the bidirectional beam function combination method [20] could be used to approximate the mode shape of the plate under any boundary conditions (i.e., simply supported, fixed, free, or any combinations) and further to analyze the dynamic characteristics.

The plate's mode shape can be expressed as

$$W_p(x, y) = \sum_{i=1}^{n}\sum_{j=1}^{n} a_{ij} X_i(x) Y_j(y), \tag{1}$$

Table 1: Physical properties of PLA [19].

Category	Unit	Value
Density	g/cm^3	1.21–1.25
Tensile strength	MPa	21–60
Ultimate strain	%	2.5–6
Elastic modulus	GPa	0.35–3.5
Glass transition temperature	˚C	45–60
Melting temperature	˚C	150–162

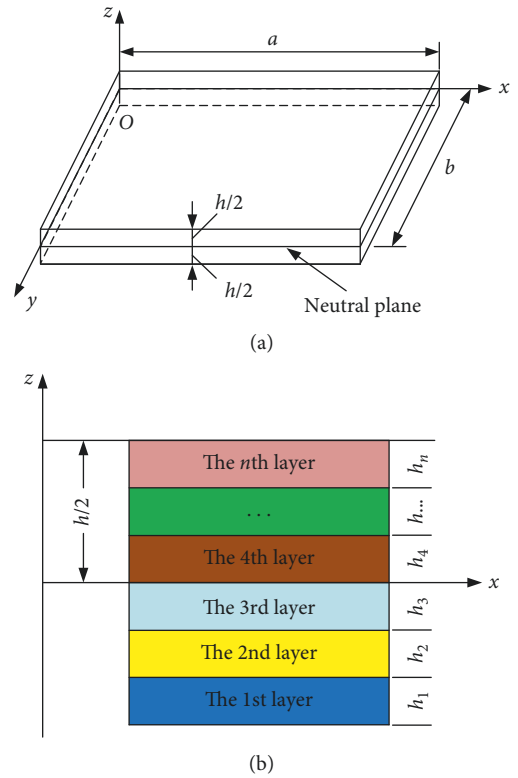

Figure 1: Physical modeling graph of the FFF plate.

where $X_i(x)$ is the i^{th} order mode shape function meeting the boundary condition in x direction, $Y_j(y)$ is the j^{th} order mode shape function meeting the boundary condition in y direction, and a_{ij} is an undetermined coefficient, which is utilized to adjust the combination of beam functions in different orders so as to make the mode shape function closer to the real mode shape of the rectangular plate.

The x-axis direction is free boundary condition, considering $X_i(x)$ as the n^{th} order's mode shape function of a free-free beam, the expression of each order mode shape is

$$\begin{aligned} X_1 &= 1, \\ X_2 &= \sqrt{3\left(1 - \frac{2x}{a}\right)}, \\ X_i &= \operatorname{ch}\frac{k_i x}{a} + \cos\frac{k_i x}{a} - \alpha_i\left(\operatorname{sh}\frac{k_i x}{a} + \sin\frac{k_i x}{a}\right), \end{aligned} \tag{2}$$

where k_i is the coefficient related to beam frequency, $k_i^4 = \omega^2(\rho A/EJ)$, ω is the circular frequency, ρ is the density,

A is the area, E is the elastic modulus, and $J = h^3/12$, α_i is the beam function coefficient, $\alpha_i = (\mathrm{ch}k_i a - \cos k_i a)/(\mathrm{sh}k_i a - \sin k_i a)$ $(i = 3, 4, 5, \ldots)$. The 1st order (X_1) shows the movement of the rigid body; the 2nd order (X_2) shows the torsion of the rigid body; and starting from the 3rd order, the mode shape is caused by the beam deformation.

In y-axis direction, the plate can be seen as a fixed-free beam, and the expression of each order's mode shape function is

$$Y_i = \mathrm{ch}\frac{k_j y}{b} - \cos\frac{k_j y}{b} - \alpha_j\left(\mathrm{sh}\frac{k_j y}{b} - \sin\frac{k_j y}{b}\right), \tag{3}$$

where k_j is the same as k_i, $\alpha_j = (\mathrm{ch}k_i b - \cos k_i b)/(\mathrm{sh}k_i b - \sin k_i b)$ $(i = 3, 4, 5, \ldots)$. The frequency coefficient [20] is detailed in Table 2.

Substitute equations (2) and (3) into equation (1), the mode shape function of the FFF plate under cantilever boundary condition is given by

$$\begin{aligned} W_p = {} & X_1 \cdot Y_1 \cdot a_{11} + X_1 \cdot Y_2 \cdot a_{12} + X_1 \cdot Y_3 \cdot a_{13} \\ & + X_2 \cdot Y_1 \cdot a_{21} + X_2 \cdot Y_2 \cdot a_{22} + X_2 \cdot Y_3 \cdot a_{23} \\ & + X_3 \cdot Y_1 \cdot a_{31} + X_3 \cdot Y_2 \cdot a_{32} + X_3 \cdot Y_3 \cdot a_{33} + \ldots. \end{aligned} \tag{4}$$

Ritz method [21, 22] was adopted to obtain the results of the inherent characteristics of the sample. It is an approximate solution method according to the energy variation principle, which could obtain the results by transforming functional extremum problem to the extremum problem of multivariate function. Due to the dynamic excitation, the plate would be deformed, producing stress and strain. Therefore, there is deformation energy varying with time existing in the plate.

The displacement can be expressed by

$$w(x, y, t) = w(x, y)\sin(\omega t + \varphi), \tag{5}$$

where $w(x, y)$ is the maximum displacement of a point on the plate, ω is the circular frequency of the plate, t is time, and φ is the initial phase.

The potential energy and kinetic energy of the plate are given separately by

$$\begin{aligned} U = {} & \frac{D}{2}\iint_A \left\{\left(\frac{\partial^2 w}{\partial x^2} + \frac{\partial^2 w}{\partial y^2}\right)^2 \right. \\ & \left. - 2(1 - v)\left[\left(\frac{\partial^2 w}{\partial x^2}\right)\left(\frac{\partial^2 w}{\partial y^2}\right) - \left(\frac{\partial^2 w}{\partial x\,\partial y}\right)^2\right]\right\} \mathrm{d}x\,\mathrm{d}y, \end{aligned} \tag{6}$$

$$T = \frac{\rho h}{2}\iint_A \left(\frac{\partial^2 w}{\partial t^2}\right)^2 \mathrm{d}x\,\mathrm{d}y, \tag{7}$$

where D is the bending stiffness, v is Poisson ratio, and ρ is the density of the sample.

Substitute the mode shape function equation (4) into equations (6) and (7), and let the partial derivative of $U_{\max} - T_{\max}$ in terms of the undetermined coefficient α_{ij} equal 0, that is

Table 2: The coefficient of beam frequency.

Boundary conditions		α_i		
$x = 0$	$x = a$	$i = 1$	$i = 2$	$i = 3$
Free	Free	0	0	4.73
Fixed	Free	1.875	4.694	7.855

$$\frac{\mathrm{d}U_{\max}}{\mathrm{d}\alpha_{ij}} - \frac{\mathrm{d}T_{\max}}{\mathrm{d}\alpha_{ij}} = 0. \tag{8}$$

The linear algebraic equation for α_{ij} is thus obtained. Set the coefficient determinant of the equation to be 0, and the circular frequency ω can be determined. According to $f = \omega/2\pi$, the natural frequency of the FFF plate can be obtained. Substitute the circular frequency into equation (4), and the mode shapes would be obtained.

2.2. Experimental Analysis

2.2.1. Sample Preparation. To determine the effect of different extrusion width on tensile property, three types of samples were fabricated by an FFF device (D-force v2). The size was determined according to ISO 527-2-2012 (International standard, plastics determination of tensile properties Part 2: test conditions for moulding and extrusion plastics). Their extrusion width (a certain width of the filament extruded from the nozzle) was separately set to 0.4, 0.3, and 0.2 mm. These samples are represented by $T_{\mathrm{E0.4\_}i}$, $T_{\mathrm{E0.3\_}i}$, and $T_{\mathrm{E0.2\_}i}$ $(i = 1\sim5)$, and the schematic is shown in Figure 2(a), with the fibers parallel to the printing platform and pointing to X direction.

For the dynamic characteristic, another three types of samples (shown in Figure 2(b)) were fabricated by the same FFF device, with the extrusion width separately being 0.4 mm (E0.4_i), 0.3 mm (E0.3_i), and 0.2 mm (E0.2_i), $i = 1\sim5$. The fibers are parallel to the printing platform, pointing to X direction (see the build direction shown in Table 3). It is noted that all the samples are made of PLA, and apart from extrusion width, the other processing parameters are set the same, such as printing speed (moving speed of the printing head during the manufacturing process) and extruder temperature (the temperature of the extruder to heat the filament to molten state). Some details are listed in Table 3.

2.2.2. Tensile Test. According to ISO 527-2-2012, the tensile tests were carried out on the samples ($T_{\mathrm{E0.4\_}i}$, $T_{\mathrm{E0.3\_}i}$, and $T_{\mathrm{E0.2\_}i}$, $i = 1\sim5$) using the testing machine (model: Shimadzu EHF-EV 200k2-040, as shown in Figure 3).

The loading rate during the test was set to 5 mm/min. Since the mechanical strength of PLA is much lower than steel, the clamping force at both ends was only set to 5 MPa in order to avoid breaking the specimen, and thereby it ensures the measurement accuracy.

2.2.3. Dynamic Test. To measure the dynamic characteristics of FFF plates, modal tests were performed on the samples

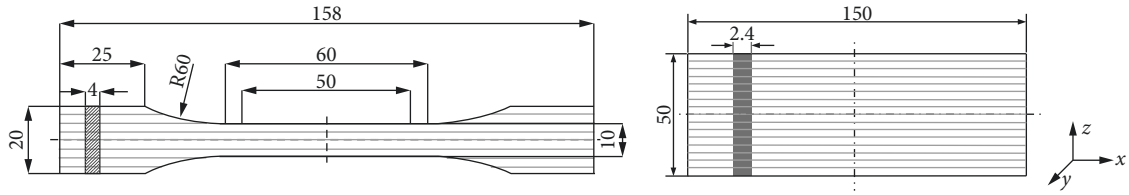

Figure 2: Two-dimensional drawing of the samples. (a) Tensile test sample; (b) dynamic test sample.

Table 3: The key processing parameter settings for the samples.

Sample (i = 1~5)	$T_{E0.4\_i}$	E0.4_i	$T_{E0.3\_i}$	E0.3_i	$T_{E0.2\_i}$	E0.2_i
Extrusion width (mm)	0.4		0.3		0.2	
Longitudinal section (mm)	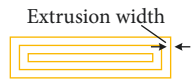		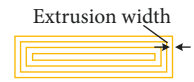		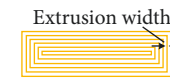	
Build direction	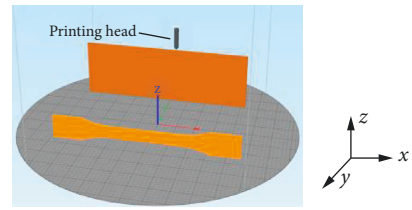			X-direction fibers (0°)		
Layer height (mm)	0.15	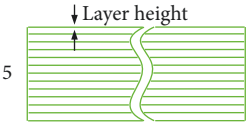				
Printing speed (mm/s)	60					
Number of contours	3	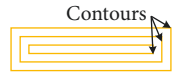	4	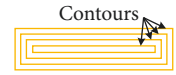	6	
Extruder temperature (°C)	200					

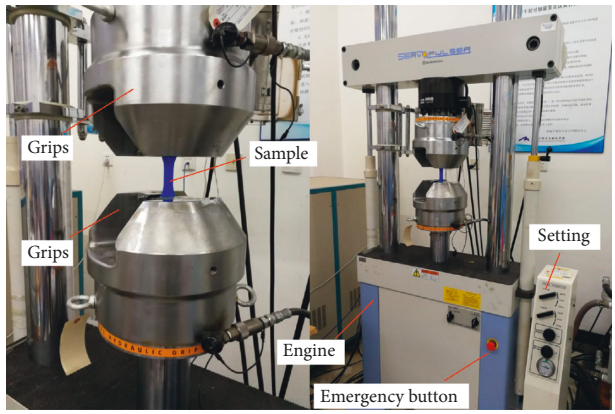

Figure 3: Tensile test machine (servo-hydraulic) and the sample.

(E0.4_i, E0.3_i, and E0.2_i, i = 1~5). Figure 4 shows the testing system. It mainly includes impact hammer (PCB 086C01), data acquisition card (NI USB 4431), and accelerometer (B&K4517, weight 0.6 g). The plates were fixed with the clamping device to be under cantilever boundary conditions, with the height of the clamping area being 20 mm. The excitation point was about 10 mm away from the bottom, as shown in Figure 4. To ensure the accuracy of the measurement, the accelerometer was successively fixed to the measuring points on the plate with large response (the top and the middle positions of the sample, avoiding the node).

During the experiment, the impulse excitation was first applied to the samples by the hammer. The dynamic response of the sample due to the excitation was then

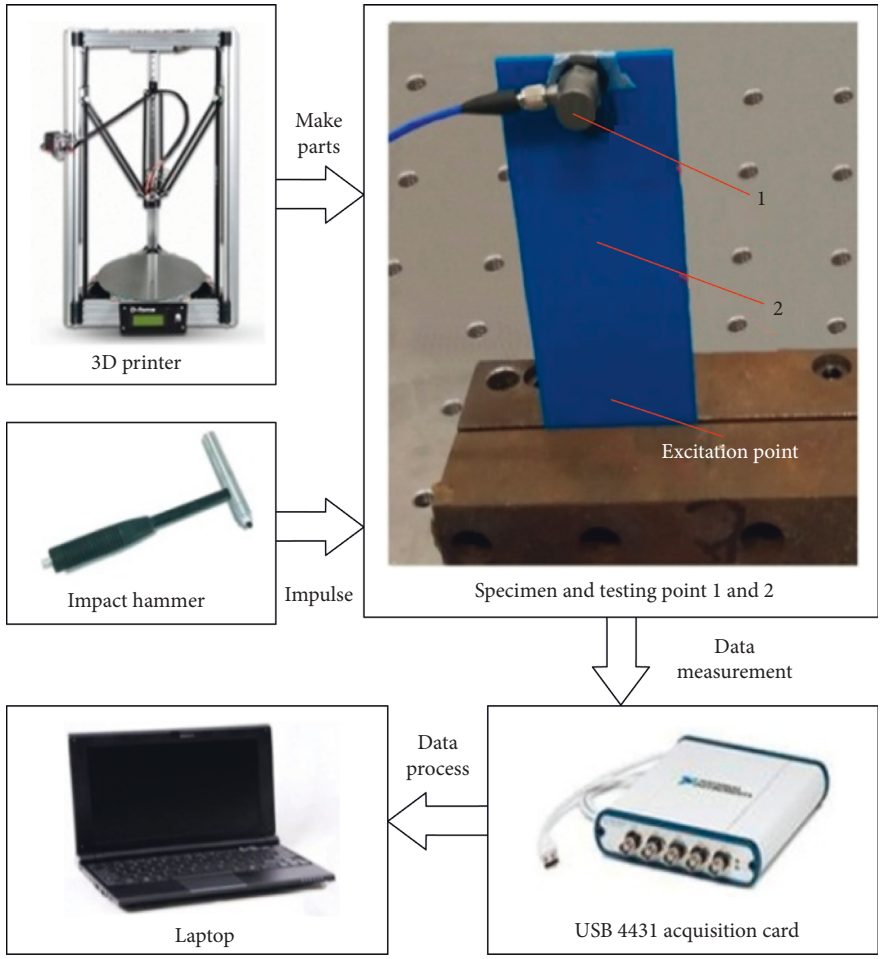

Figure 4: Testing system for determining the dynamic characteristics of FFF plates.

Table 4: Material properties of FFF plates.

Sample	Average elastic modulus (MPa)	Average shear modulus (MPa)	Weight (g)	Average density (g/cm^3)	Poisson ratio
E0.4	18.8	7.23		0.92	
E0.3	18.5	7.12	17.0	0.91	0.36
E0.2	18	6.92		0.91	

measured by the accelerometer. At the same time, the real-time excitation and response signal was collected through the data acquisition card. In order to obtain the mode shape of the sample, the MISO (multiple-input single-output) method was adopted, meaning that the accelerometer was fixed at the position with large response and the other measuring positions were excited separately in turn. For each sample, 10 groups of tests were completed (150 groups of measured data obtained in total), further ensuring the accuracy of the measurements.

3. Results and Discussions

Based on Hooke's law, the elastic modulus of the samples was obtained. According to the equation $G = E/2(1 + \upsilon)$, the FFF plates' shear elastic modulus could be determined, where υ is poisson ratio and $\upsilon = 0.36$ [19]. The samples were weighted using the electrical analysis balance (FA2004), whose accuracy is 0.1 mg. Together with the plates' three-dimensional size, the density of each sample was determined.

Table 4 summarizes the average material properties of the sample for dynamic test. It can be seen that the wider the extrusion width is, the larger the material property of the corresponding samples will be. This can be explained that when the extrusion width increases, the bonding area between adjacent extruded filaments is increased, leading to the improvement of bonding strength. There would be fewer thermal cycles and nonuniform thermal gradients, leading to fewer distortions and deformations of the extruded filament, and thus better bonding quality. In addition, the bonding gap between the cross section's filaments would decrease, generating fewer defects such as internal pores and void structures. Therefore, the material property of the sample is improved with the increase of extrusion width.

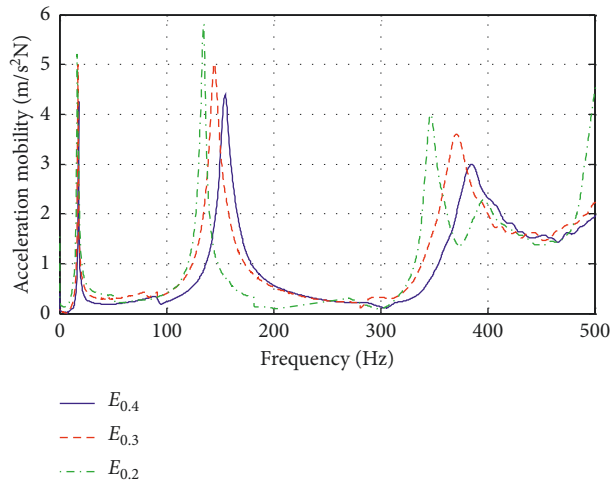

Figure 5: The average measured frequency response curves of the dynamic test samples.

Table 5: The resonant response of the samples fabricated with different extrusion width.

Sample	Average resonant response (m/s^2N)		
	1st order	2nd order	3rd order
E0.4	4.3	4.4	3.0
E0.3	5.0	5.0	3.6
E0.2	5.2	5.8	4.0

Figure 5 presents the average measured frequency response curves of the FFF samples fabricated with different extrusion widths, whose values are separately 0.4, 0.3, and 0.2 mm. Although the devices attached on the sample are lightweight, they can influence the exact values of the dynamics characteristic parameters to some extent. But the corresponding qualitative analysis is still reliable as the influence has the same trend. They are not the origin of the spectral variations. Therefore, the effect of the accelerometer and cable on the sample's dynamics characteristics was able to be ignored.

The results are detailed in Table 5. It can be seen that Sample E0.4 has the highest natural frequency and lowest values of resonant response (due to the impulse excitation), meaning that the antivibration capability is the best compared with the other two types of samples. As mentioned above, this is because increasing extrusion width will improve the forming quality of the samples. Therefore, the sample's dynamic characteristic (i.e., antivibration capability) will be improved if the extrusion width is increased.

To validate the theoretical model, the predicted natural frequency and mode shapes are compared with the measurements. Details are shown in Table 6. It can be seen from the comparison that the predictions agree well with the measurements. The discrepancy between predicted and measured natural frequency is in the range of 7.2%–13.4%. The predicted mode shapes are the same as the measured ones. The 1st order mode shape is the 1st order bending vibration, the 2nd order one is the 1st order torsional vibration, and the 3rd order one is the 2nd order bending vibration. Therefore, the theoretical model set up based on the bidirectional beam function combination method can give reliable predictions in inherent characteristic (i.e., natural frequency and mode shape) of the FFF plate. As it was set up closely to the actual situation (considering the effect of orthogonal anisotropy relying on the classical laminated plate theory) and solved by the reliable algorithm (Ritz method).

In addition, larger extrusion width mainly leads to the increase in elastic modulus of the sample, which would enhance the structural stiffness of the plate according to equation (6), and this will lead to better dynamic characteristics. According to the basic theory of mechanical vibration, larger structural stiffness generally means higher natural frequencies. As can be seen from the table, the sample fabricated with the extrusion width being 0.4 mm has the largest elastic modulus (18.8 MPa) among the three types of samples; the corresponding natural frequency is the highest, with the first three measured natural frequencies being 18 Hz, 154.9 Hz, and 384.8 Hz. For Sample E0.2, these values are separately 16.1 Hz, 134.2 Hz, and 346 Hz, with the elastic modulus being 18 MPa. Since all the samples are thin plate structure, the structural characteristic is not changed or influenced by different extrusion widths and the corresponding mode shapes are kept the same.

Although the theoretical modeling makes it possible to analyze and predict the inherent characteristics of the plates, errors inevitably occur and they may come from two aspects, theoretical modeling and experimental testing. In the modeling, the sample was regarded as an

Table 6: The predicted and measured inherent characteristics of the samples.

Category	Extrusion width	Order 1st	Order 2nd	Order 3rd
Average measured natural frequency A (Hz)	0.4 mm	18.0	154.9	384.8
	0.3 mm	17.1	145.6	371.1
	0.2 mm	16.1	134.2	346.0
Average predicted natural frequency B (Hz)	0.4 mm	19.3	170.1	429.4
	0.3 mm	18.5	159.6	416.0
	0.2 mm	17.6	148.6	392.4
Error (%) $\lvert B - A\rvert/A$	0.4 mm	7.2	9.8	11. 6
	0.3 mm	8.2	9.6	12.1
	0.2 mm	9.3	10.7	13.4
Measured mode shape			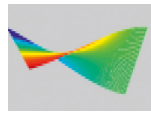	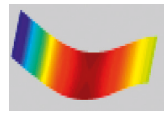
Predicted mode shape		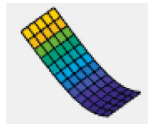	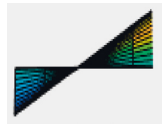	

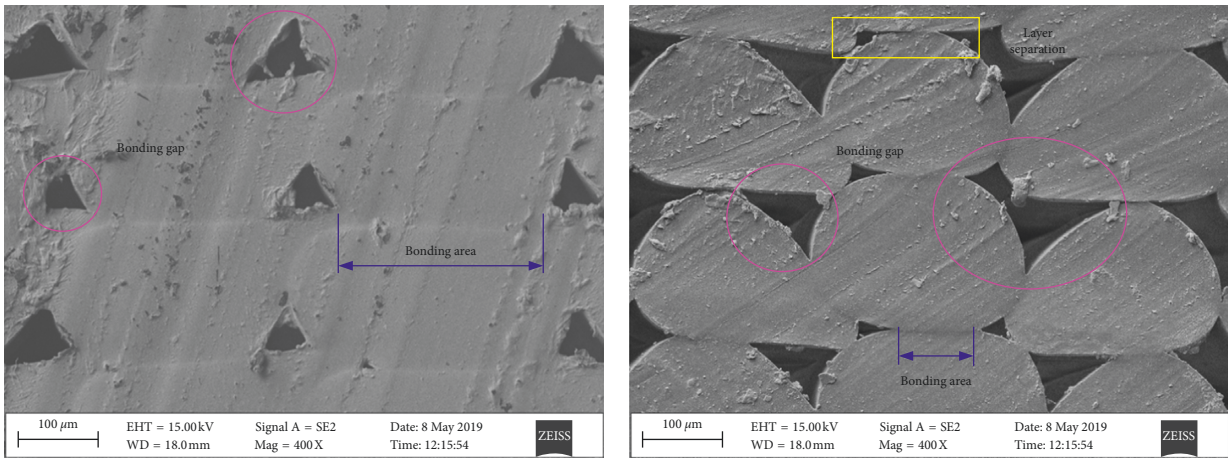

(a) (b)

Figure 6: SEM micrograph of the sample's cross section with extrusion width being (a) 0.4 and (b) 0.2 mm.

integral structural plate; the stress and strain between layers were not taken into account. Furthermore, the effects of transverse shear stress, interface defect, residual stress, and the dispersion of material parameters were ignored. The error also occurred in the experiment, for example, the clamping extent of the fixture (boundary conditions) and the testing instrument sensitivity drift would cause adverse influence.

From the microscopic view, the bonding area between adjacent extruded filaments will be decreased when the extrusion width decreases (as shown in Figure 6), leading to the deterioration of bonding strength. There would be more thermal cycles and more nonuniform thermal gradients, leading to more distortions and deformations of the extruded filament, which is a major reason for the bonded layers' poor quality [18], and thus worse bonding quality. In addition, it can be seen from Figure 6 that decreasing extrusion width would increase the bonding gap between the filaments of the cross section, generating more defects such as layer separations, internal pores, and void structures. Therefore, decreasing extrusion width will deteriorate the mechanical property and dynamic performance of the FFF product.

Figure 7 provides the surface SEM observation of the samples fabricated with the extrusion width being 0.4 and 0.2 mm, respectively. It is a side view of the sample, showing the microscope details of the layer height. From the comparison, it can be seen that as the extrusion width is reduced down to 0.2 mm, there are more distortions

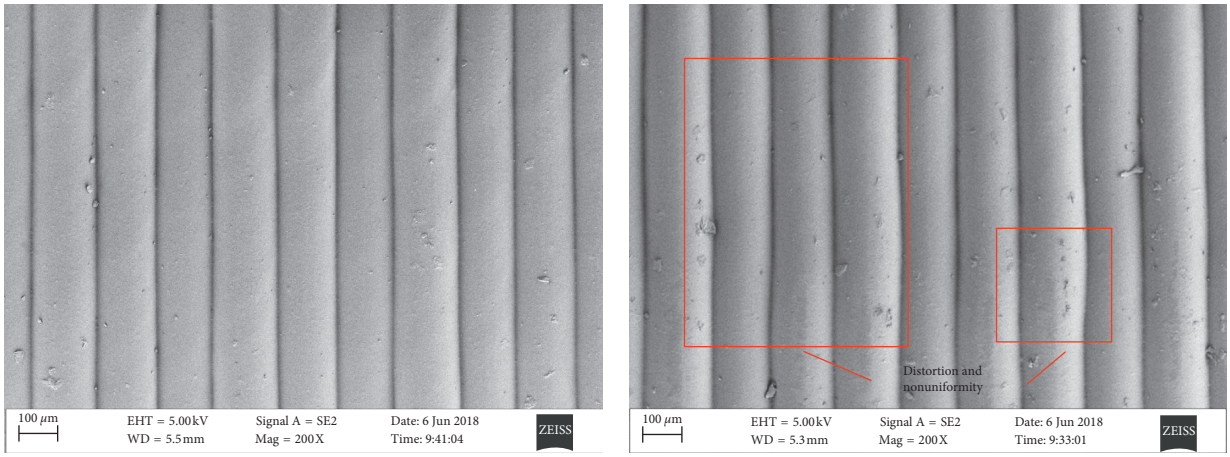

(a) (b)

Figure 7: SEM micrograph of the side surface of the sample fabricated with extrusion width being (a) 0.4 and (b) 0.2 mm.

and nonuniformities in the sample, resulting in poorer bonding quality between extruded filaments. Therefore, the mechanical and dynamical characteristics of the sample will decrease with the reduction of extrusion width.

4. Conclusions

Combining theory with experiment, this paper studied the inherent characteristic of FFF plates under cantilever boundary conditions and quantified the effect of extrusion width. It can be concluded that different extrusion widths can lead to the difference in material property of the FFF sample. The material properties are improved with the increase of extrusion width. The dynamic characteristic (i.e., antivibration capability) of the sample will be improved if the extrusion width is increased. Compared with the measurements, the theoretical model set up based on the bidirectional beam function combination method can reliably predict the natural frequency and mode shape of the FFF plate, with the error within the confidence level. The greater the material property of the sample is, the higher the corresponding natural frequency will be. Since the structural characteristic is not changed or influenced by different extrusion widths, the mode shapes are kept the same. The SEM shows that the mechanical and dynamical characteristics of the FFF plate are deteriorated as the extrusion width decreases. However, the study on more processing parameters is recommended to further confirm the theoretical model and to quantify their effect on FFF parts' dynamic characteristics. This paper provides theoretical basis and technical support for further research in improving the dynamic performance of FFF products.

Data Availability

The experimental and theoretical data used to support the findings of this study are available from the corresponding author upon request.

Conflicts of Interest

The authors declare that they have no conflicts of interest.

Acknowledgments

The work described was supported by the National Natural Science Foundation of China (51705068) and the Fundamental Research Funds for the Central Universities (N180703009).

References

[1] O. A. Mohamed, S. H. Masood, and J. L. Bhowmik, "Optimization of fused deposition modeling process parameters: a review of current research and future prospects," *Advances in Manufacturing*, vol. 3, no. 1, pp. 42–53, 2015.

[2] H. Rezayat, W. Zhou, A. Siriruk, D. Penumadu, and S. S. Babu, "Structure-mechanical property relationship in fused deposition modelling," *Materials Science and Technology*, vol. 31, no. 8, pp. 895–903, 2015.

[3] C. A. Griffiths, J. Howarth, G. De Almeida-Rowbotham, and A. Rees, "A design of experiments approach to optimise tensile and notched bending properties of fused deposition modelling parts," *Proceedings of the Institution of Mechanical Engineers, Part B: Journal of Engineering Manufacture*, vol. 230, no. 8, pp. 1502–1512, 2016.

[4] M. Rinaldi, T. Ghidini, F. Cecchini, A. Brandao, and F. Nanni, "Additive layer manufacturing of poly (ether ether ketone) via FDM," *Composites Part B: Engineering*, vol. 145, pp. 162–172, 2018.

[5] S. Hwang, E. I. Reyes, K.-S. Moon, R. C. Rumpf, and N. S. Kim, "Thermo-mechanical characterization of metal/polymer composite filaments and printing parameter study for fused deposition modeling in the 3D printing process," *Journal of Electronic Materials*, vol. 44, no. 3, pp. 771–777, 2015.

[6] J. Torres, J. Cotelo, J. Karl, and A. P. Gordon, "Mechanical property optimization of FDM PLA in shear with multiple objectives," *JOM*, vol. 67, no. 5, pp. 1183–1193, 2015.

[7] S. Maleksaeedi, H. Eng, F. E. Wiria, T. M. H. Ha, and Z. He, "Property enhancement of 3D-printed alumina ceramics

using vacuum infiltration," *Journal of Materials Processing Technology*, vol. 214, no. 7, pp. 1301–1306, 2014.

[8] O. S. Es-Said, J. Foyos, R. Noorani, M. Mendelson, R. Marloth, and B. A. Pregger, "Effect of layer orientation on mechanical properties of rapid prototyped samples," *Materials and Manufacturing Processes*, vol. 15, no. 1, pp. 107–122, 2000.

[9] M. Altan, M. Eryildiz, B. Gumus, and Y. Kahraman, "Effects of process parameters on the quality of PLA products fabricated by fused deposition modeling (FDM): surface roughness and tensile strength," *Materials Testing*, vol. 60, no. 5, pp. 471–477, 2018.

[10] M. K. Kim, I. H. Lee, and H.-C. Kim, "Effect of fabrication parameters on surface roughness of FDM parts," *International Journal of Precision Engineering and Manufacturing*, vol. 19, no. 1, pp. 137–142, 2018.

[11] E. G. Gordeev, A. S. Galushko, and V. P. Ananikov, "Improvement of quality of 3D printed objects by elimination of microscopic structural defects in fused deposition modeling," *PLoS One*, vol. 13, no. 6, Article ID e0198370, 2018.

[12] M. Yuan and D. Bourell, "Quality improvement of optically translucent parts manufactured from LS and SL," *Rapid Prototyping Journal*, vol. 22, no. 1, pp. 87–96, 2016.

[13] M. A. Caminero, J. M. Chacón, I. García-Moreno, and J. M. Reverte, "Interlaminar bonding performance of 3D printed continuous fibre reinforced thermoplastic composites using fused deposition modelling," *Polymer Testing*, vol. 68, pp. 415–423, 2018.

[14] A. Boschetto and L. Bottini, "Design for manufacturing of surfaces to improve accuracy in fused deposition modeling," *Robotics and Computer-Integrated Manufacturing*, vol. 37, pp. 103–114, 2016.

[15] H. Prüß and T. Vietor, "Design for fiber-reinforced additive manufacturing," *Journal of Mechanical Design*, vol. 137, no. 11, p. 111409, 2015.

[16] A. Arivazhagan and S. Masood, "Dynamic mechanical properties of ABS material processed by fused deposition modelling," *International Journal of Engineering Research and Applications*, vol. 2, no. 3, pp. 2013-2014, 2012.

[17] O. A. Mohamed, S. H. Masood, J. L. Bhowmik, M. Nikzad, and J. Azadmanjiri, "Effect of process parameters on dynamic mechanical performance of FDM PC/ABS printed parts through design of experiment," *Journal of Materials Engineering and Performance*, vol. 25, no. 7, pp. 2922–2935, 2016.

[18] O. A. Mohamed, S. H. Masood, and J. L. Bhowmik, "Investigation of dynamic elastic deformation of parts processed by fused deposition modeling additive manufacturing," *Advances in Production Engineering & Management*, vol. 11, no. 3, pp. 227–238, 2016.

[19] S. Farah, D. G. Anderson, and R. Langer, "Physical and mechanical properties of PLA, and their functions in widespread applications - a comprehensive review," *Advanced Drug Delivery Reviews*, vol. 107, pp. 367–392, 2016.

[20] V. L. Berdichevsky, "Theory of elastic plates and shells," in *Variational Principles of Continuum Mechanics: II. Applications*, pp. 589–714, Springer, Berlin, Germany, 2009.

[21] K. K. Pradhan and S. Chakraverty, "Free vibration of Euler and Timoshenko functionally graded beams by Rayleigh-Ritz method," *Composites Part B: Engineering*, vol. 51, pp. 175–184, 2013.

[22] R. B. Bhat, "Natural frequencies of rectangular plates using characteristic orthogonal polynomials in Rayleigh-Ritz method," *Journal of Sound and Vibration*, vol. 102, no. 4, pp. 493–499, 1985.